Paper published in Proc. of 28th International Congress on Applications of Lasers & Electro-Optics (ICALEO 2009)

CLOSED LOOP CONTROL OF LASER WELDING PROCESSES USING CELLULAR NEURAL NETWORK CAMERAS - EXPERIMENTAL RESULTS

Paper (P137)

F. Abt[1], A. Blug[2], L. Nicolosi[3], F. Dausinger[4], R. Weber[5], R. Tetzlaff[3], D. Carl[2], H. Höfler[2]

[1]FGSW Forschungsgesellschaft für Strahlwerkzeuge gGmbH, Stuttgart, Germany

[2]IPM Fraunhofer Institut für Physikalische Messtechnik, Freiburg, Germany

[3]Technische Universität Dresden, Dresden, Germany

[4] Dausinger + Giesen GmbH, Stuttgart, Germany

[5]IFSW Institut für Strahlwerkzeuge, Stuttgart, Germany

Abstract

Today, image processing using coaxial camera setups is used to monitor the quality of laser material processes such as laser welding, cutting or ablation. This article shows the potentials of a sensing system for the next step: A closed loop control of a full penetration keyhole welding process.

With "Cellular Neural Networks" (CNN) it is possible to integrate processor elements in the electronic circuitry of CMOS cameras resulting in a Single-Instruction-Multiple-Data (SIMD)-architecture on the camera chip itself. Such pixel parallel systems provide extremely fast real-time image processing. This allows it to employ algorithms for image processing which are widely independent of the exact process parameters, reducing the adaption effort for different applications, compared to photo diode systems.

A closed loop control system was implemented into a commercially available laser welding machine. This system uses a CNN based camera surveying the contour of the full penetration hole with a control frequency of up to 14 kHz for linear weldings. As a result the system reaches and holds the full penetration state automatically. A more detailed description of the control system and the used algorithms is given in [1].

This paper presents achievable welding results in scanner-based remote welding processes, with a new direction independent algorithm. To demonstrate the capabilities of the closed loop control, welding experiments with changing process conditions were carried out.

Introduction

CNN have been introduced by Chua and Yang in 1988 [2] to be employed in such areas like image processing and pattern recognition. The basic circuit unit of CNNs is called a cell. Each cell can directly interact with its neighbouring cells since it is connected to them, and indirectly with the other cells due to propagation effects caused by the continuous-time dynamics of the CNN. Together with the memory of each cell the CNN is a network in space (neighbour cells) and time (previous states in the memory). An example of a two-dimensional CNN is shown in Fig. 1.

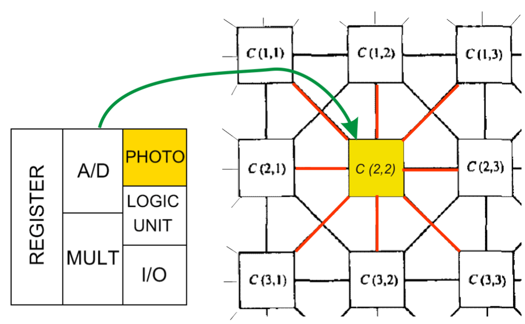

Fig. 1: 2D CNN scheme: each cell is directly connected with its neighbouring cells. Each of the cells consists of a photo sensitive area and a surrounding analogue processor unit.

The CNN analogue implementation allows to perform parallel processing since each pixel has its own processor element and the cell interaction occurs in a really short time determined by the time constant of the single cell. This makes the CNN one of the best approaches for real-time image processing. A more detailed description of the CNN-technology is given in [2], [3], [4] and [5].

Paper published in Proc. of 28th International Congress on Applications of Lasers & Electro-Optics (ICALEO 2009

The laser welding process

The main focus of this paper is on keyhole welding of zinc-coated steel in an overlap-joint with solid state lasers. This is a very common process in the automotive industry, especially in car body welding. Most of the experiments in this paper were carried out on zinc-coated steel sheets with thicknesses between 0.7 and 2.5 mm.

A very important quality feature is the so called full penetration of the joining partners. The full penetration is achieved, when the laser beam fully penetrates both joining partners and leaves a clearly visible seam on the upper and lower side. This process state ensures a proper cross section of the weld seam and strong connection of the metal sheets.

Fig. 2 shows the sketch of a longitudinal section of the laser welding process and the resulting image of a coaxial camera in the near infrared spectrum. As one can see in Fig. 2, the full penetration quality feature is directly visible in the camera image as a dark area following the interaction zone of the laser. This is because the capillary is fully open at the bottom of the joining partners and thus there is no molten material that emits thermal radiation in this area. This was also observed in previous publications [6], [7] and [8].

Experimental setup

The welding experiments were carried out with a 2D laser scanner setup. The laser source for the experiments is a 6 kW, 1030 nm Trumpf TruDisk 6002 Yb:YAG thin disk laser with a 200 µm transport fibre. The laser scanner used – a Trumpf PFO-33 – was equipped with a 450 mm focusing optic which resulted in a focal diameter of 600 µm.

The Eye-RIS CNN-camera system is adapted to the scanner optics through a 90° beam splitter, see Fig. 3. Thus the camera perspective is coaxial to the laser beam. This allows an invariant field of view regardless of the scanner position. It is necessary to use an aligned lens system in order to achieve an appropriated region of interest (ROI) for the camera. For the experiments a lens system consisting of three achromatic lenses was designed to achieve an optical magnification β of about 4.6. In combination with an optical band-pass filter – transmission from 820 nm up to 980 nm – camera images with high quality can be achieved [3].

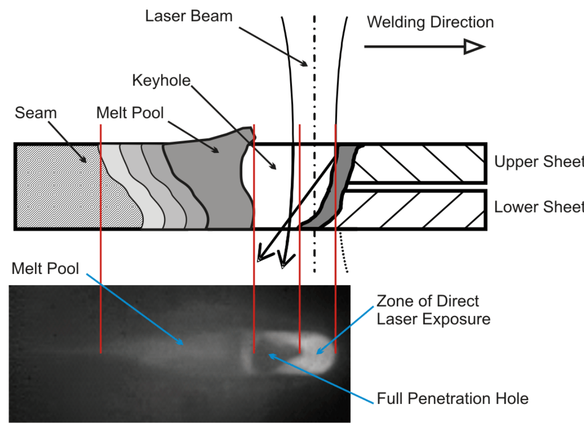

Fig. 2: Schematics of a welding process in an overlap-joint and the corresponding camera image.

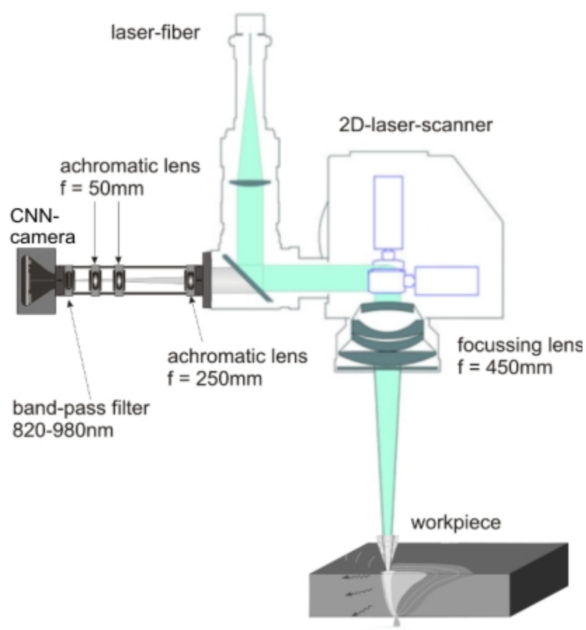

Fig. 3: Optical setup with the laser scanner, the CNN-camera and the optical imaging system.

Hardware and algorithms

Camera Hardware

The CNN-camera used for the welding experiments is an Anafocus Eye-RIS v1.2 camera with the new Q-Eye chip [9]. The Q-Eye is a quarter CIF resolution fully programmable smart image sensor. It consists of 176 x 144 cells, each containing a processor merged with an optical sensor, memory circuitry and interconnections to the 8 neighbouring cells. This means that each pixel can both sense the corresponding spatial sample of the image and process this information in close interaction with other pixels.

Paper published in Proc. of 28th International Congress on Applications of Lasers & Electro-Optics (ICALEO 2009

Besides the Q-Eye focal plane processor, the Eye-RIS camera system consists of an additional FPGA based NIOS II processor by Altera to control the operation of the whole vision system and to analyze the information output of the Q-Eye chip performing all the decision-making and actuation tasks.

Direction independent algorithm

In former publications [3], [4], [10], some different dilation based algorithms were shown. A serious limitation of these algorithms is the fact that the welding direction has to be kept constant and it must be a priori known. To overcome this limitation a new direction independent algorithm was developed, the so called omnidirectional algorithm [1], [11].

The omnidirectional algorithm is not longer based on dilation operations rather on opening and closing operations. The opening operation is basically an erosion followed by a dilation to delete small objects. The closing operation instead is a dilation followed by an erosion to fill up small holes. Opening and closing are also neighbourhood based operations and thus they can be efficiently run on CNN hardware.

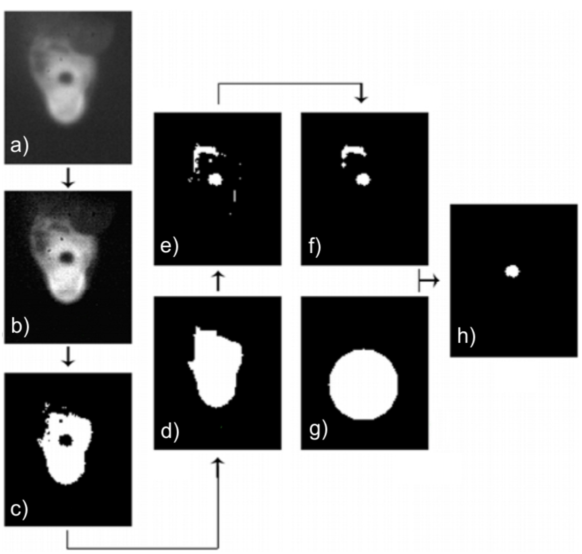

Fig. 4: Direction independent image processing algorithm. The grey-value source image a) is filtered b) and binarized c). Holes are removed by morphological closings d) and a difference-images created e).The noise is removed by morphological openings f) and a mask g) is applied to obtain the resulting image with only the pixels in the hole area left h) [11].

Fig. 4 shows the flow chart of this algorithm. The grey value source image (8 bit colour depth) a), given by the illumination of the pixels, is filtered with a sharpen-filter to enhance the contrast of the image. This results in the grey value image b). This image is binarized with a global threshold, as already shown in [12], resulting in the binary image c). All holes in the white structure are removed by morphological closing operations which lead to the solid white structure in the binary image d). A difference image e) between d) and c) is created by logical operations (XOR and AND). To remove the noise in e) morphological opening operations are performed which lead to a clean binary image f). To remove all white pixels that are not belonging to the full penetration hole, a circular mask g) is applied. The result of the algorithm is the binary image h) that only contains the white pixels belonging to the full penetration hole.

Automatic mask builder

The mask builder for the direction independent algorithm works in general like the older mask builders for the linear algorithms described in [3], [10] and [11]. The main difference is the shape of the mask. Instead of a rectangular mask the mask for the direction independent algorithm is circular. The circular shape of the mask ensures that the noise is removed independent of the welding direction as shown in Fig. 4.

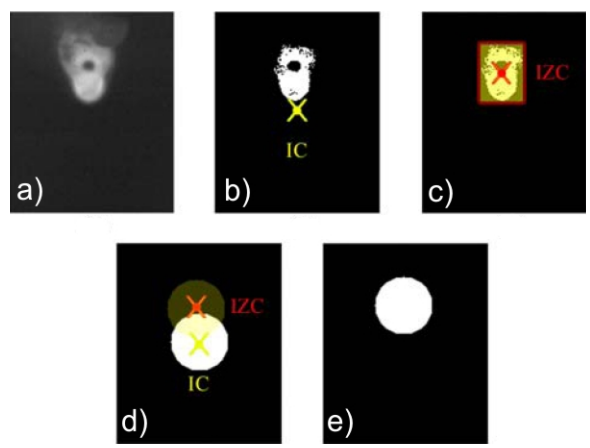

Fig. 5: Mask builder for direction independent algorithm. The grey-value source image a) is binarized b) and the interaction zone centre IZC is calculated c). The initial mask at the image centre IC is moved to the IZC position d). The final mask for the process is shown in e).

The mask is generated at the beginning of each process. As shown in Fig. 5, the initial grey value image a) is binarized with a global threshold as described above b). Afterwards the interaction zone centre IZC and the image centre IC is calculated c).

Paper published in Proc. of 28th International Congress on Applications of Lasers & Electro-Optics (ICALEO 2009

The initial mask is then moved from IC to IZC d), which leads to the final mask e) that is used for the whole weld seam.

Control system

As mentioned above, this paper deals with an algorithm implementation for closed loop tests; i.e. the CNN-camera system controls the laser welding machine. The available hardware therefore essentially consists of the Eye-RIS v1.2 CNN-camera, a numerically controlled (NC) machine, the laser source and the interface board. The NC machine is responsible for safety interlocks, laser ON/OFF signals and movement. The laser power is controlled by an analogue voltage between 0 and 10 V which corresponds to 0 – 100 % of the laser power. The interface board was built in order to receive a digital START/STOP signal from the NC machine and to control the laser power according to the pulse width modulation (PWM) signal received from the CNN-camera. A more detailed description of the system is given in [1]

The cycle time of the whole control algorithm is about 140 µs which leads to a control frequency of 7 kHz [11]. This includes all necessary steps from image acquisition over image processing to the generation of the control signal.

Experimental Results

As described above, the real-time control test employed the full penetration quality feature. Therefore, full penetration is detected by the presence or absence of the dark area behind the laser interaction zone, as described in previous chapters. The actuating variable used was the laser power. The advantages of this actuating variable are the high dynamic of up to 10 kHz for Trumpf laser systems and the fact that it can be controlled by a simple analogue signal of 0 – 10 V corresponding to a laser power output of 0 – 100 %.

As further described in the chapters above, we were able to reach a control frequency of about 7 kHz with the direction independent algorithm. This was achieved without saving the camera images, which would have dropped the control frequency to approximately 3 kHz. Some of the experiments were carried out with the linear 1-sided algorithm that reaches a control frequency of 13.8 kHz [3].

The resulting benefits are described in the following subchapters. Most of the experiments were performed with uncleaned work pieces to have a situation comparable to industrial production lines. This might lead in some cases to higher smoke residue and spatter ejection.

Comparison controlled vs. uncontrolled

The conventional way to achieve a proper full penetration weld is to regulate laser power or feed rate until full penetration is reached and add 10 % laser power as a safety factor.

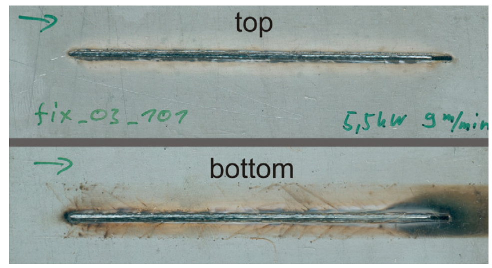

Fig. 6: Uncontrolled full penetration weld with 10 % factor of safety. Parameters are v = 9 m/min, P = 5.5 kW, zinc coated steel 2 x 0.7 mm with 0.1 mm gap in an overlap joint [3] (cleaned sheets).

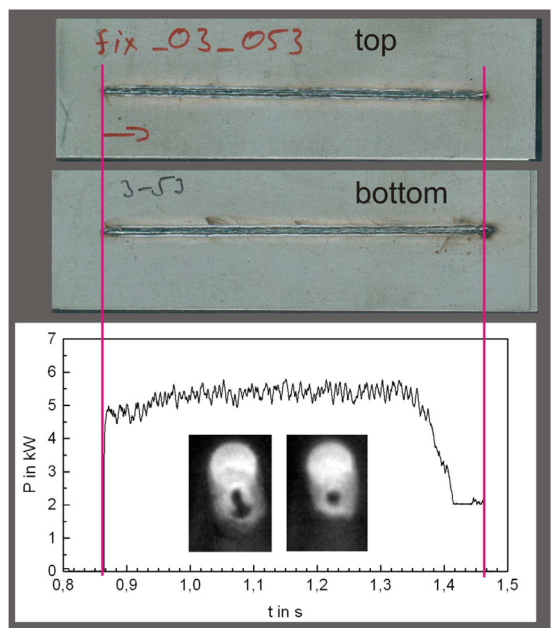

Fig. 7: Controlled full penetration weld of zinc coated steel 2 x 0.7 mm with 0.1 mm gap at a feed rate of v = 9 m/min including two exemplarily camera pictures of a good full penetration state [3].

Such a conventional uncontrolled full penetration weld is shown in Fig. 6. Typical for this process is the significant contamination of the bottom side of the joining partners with smoke residue and spatters. Furthermore, there are usually significant craters or even holes present especially at the end of the weld

Paper published in Proc. of 28th International Congress on Applications of Lasers & Electro-Optics (ICALEO 2009

seam due to the deceleration of the machine axis at the end of the welding process.

With the controlled full penetration welding process one can see a completely different behaviour (Fig. 7). Notable is the almost complete absence of smoke residue on the bottom side of the joining partners and the reduced spatter traces. It is also visible that the Eye-RIS control system reduces the laser power automatically at the end of the weld seam when the feed rate decreases to a halt. This reduces the formation of craters and holes at weld termination [3].

Laser power adaption to feed rate

The adaption of the laser power to the feed rate was tested by welding the same material at changing feed rates between 3 m/min and 9 m/min. The total length of the linear seam is 80 mm, but every 20 mm the feed rate is changed with an acceleration of 4 m/s² in steps of 2 m/min on sheets with a constant thickness of 2 x 0.9 mm and a gap of 0.2 mm. The algorithm used was the omnidirectional algorithm with a control frequency of 7 kHz As Fig. 8 illustrates, the laser power was adjusted properly by the control system to the particular feed rate. Fig. 9 shows the corresponding weld seams of the speed variation. The full penetration state was reached and maintained in all cases.

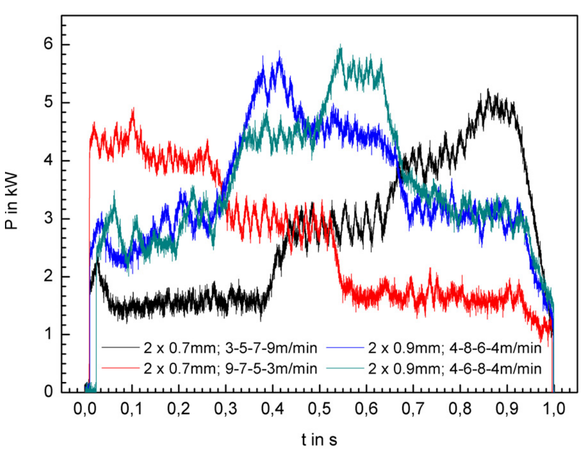

Fig. 8: Controlled full penetration weld of zinc coated steel 2 x 0.7 mm and 2 x 0.9 mm with 0.1 mm and 0.2 mm gap at different feed rates between 3 m/min and 9 m/min (omnidirectional algorithm).

The direct comparison of the omnidirectional algorithm and the linear 1-sided algorithm [3] shows that the behaviour is similar and the controlled power levels are the same for both algorithms, see Fig. 10. The only differences are visible in the rise times since the control frequency of the omnidirectional algorithm in this experiment was 7 kHz compared to the 13.8 kHz of the 1-sided algorithm.

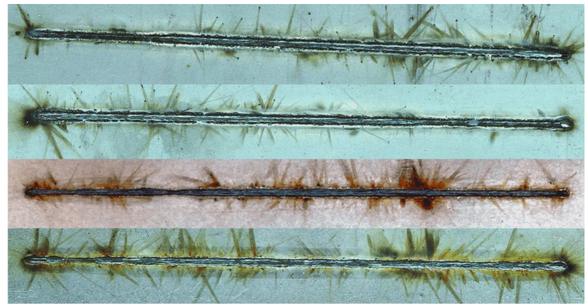

Fig. 9: Corresponding weld seams (bottom side) of the feed rate variation. From top to bottom: 2 x 0,7 mm, gap 0.1 mm; 3-5-7-9 m/min and 9-7-5-3 m/min. 2 x 0.9 mm, gap 0.2 mm; 4-8-6-4 m/min and 4-6-8-4 m/min. The welding speed changes every 20 mm (omnidirectional algorithm).

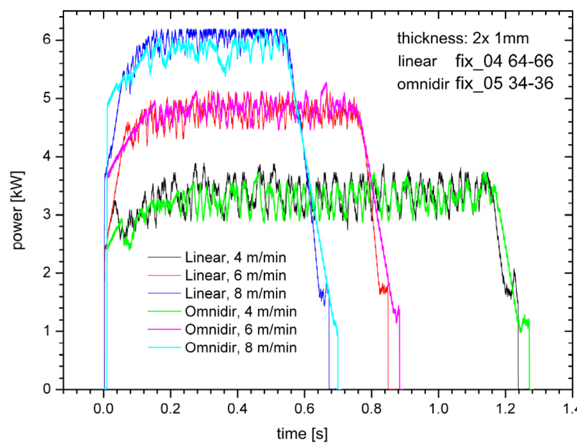

Fig. 10: Comparison of onmidirectional algorithm and the linear 1-sided algorithm described in [3].

Laser power adaption to material thickness

Experiments with changing thickness of the top sheet were carried out to test the ability of the control system to maintain the full penetration at variable material thicknesses of the joining partners.

The 1-sided algorithm reached control frequencies of about 13.8 kHz, Fig. 11 shows the positive step response of the control system to a change in the material thickness. The position of the thickness changing is marked in the diagram to measure the necessary time to change the laser power. With the control time and the power difference, it is possible to calculate the effective control speed of the system. For the experiments in Fig. 11, an effective control speed between 23 kW/s and 39 kW/s was achieved.

Paper published in Proc. of 28th International Congress on Applications of Lasers & Electro-Optics (ICALEO 2009

The effective control speed refers to the achievement of average power levels, not to the maximum power gradient, that is approximately 165 kW/s.

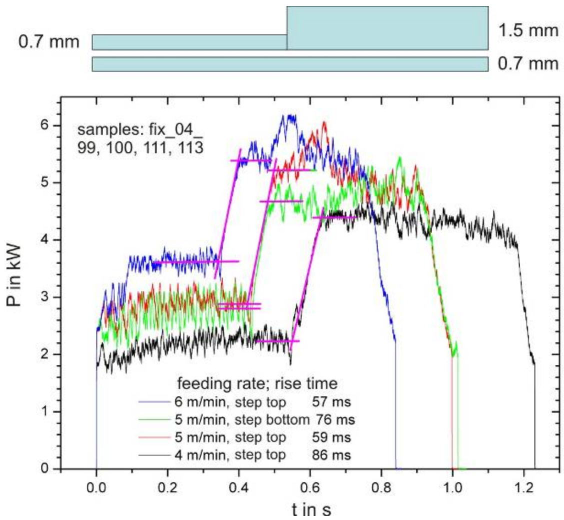

Fig. 11: Controlled full penetration weld of zinc coated steel. The material thickness changes form 2 x 0.7 mm to 0.7 mm + 1.5 mm in the middle of the weld seam. The gap is 0.1 mm in all cases [14]. (linear 1-sided algorithm)

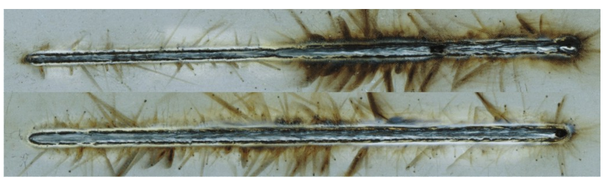

Fig. 12: Bottom sides of weld seams with 0.7 mm bottom sheet and thickness change from 0.7 mm to 1.5 mm in the top sheet in the middle of the seam. Top: fix_04_099 at 5 m/min, bottom: fix_04_113 at 6 m/min [14]. (linear 1-sided algorithm)

Exemplarily Fig. 12 shows the weld seams of two of the experiments out of Fig. 11. The full penetration was reached and maintained across the thickness step in the middle of the seam. The quality of the top and bottom side is good, without holes and penetration losses [14].

The reduced control frequency of the omnidirectional algorithm compared to the 1-sided algorithm leads to a smaller power gradient. Thus the height of the step function is reduced for this experiment.

The welding experiments in Fig. 13 have a constant feed rate of 4 m/min and a step in the top sheet from 0.7 mm to 1.0 mm. The bottom sheet was 0.7 mm in thickness with a gap of 0.1 mm. The power levels for the different stack heights are the same regardless of the direction in which the step was welded. Only in one case when starting on the thick side of the work piece, there were some power fluctuations unknown in their causation.

The bottom side of both weld seams are shown in Fig. 14. The algorithm was able to reach and hold the full penetration over the entire weld seam. Only minor irregularities are visible on the bottom side of the weld seams.

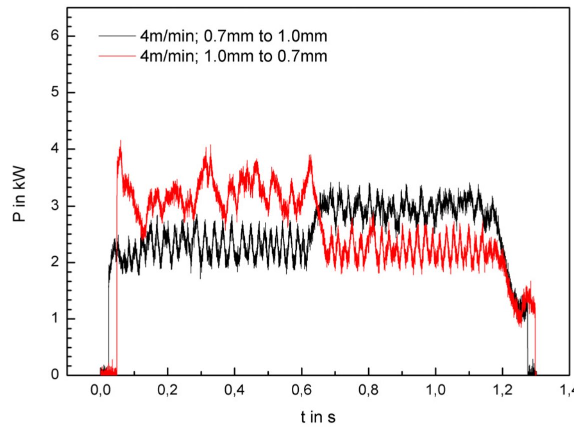

Fig. 13: Controlled full penetration weld of zinc coated steel. The material thickness changes form 2 x 0.7 mm to 0.7 mm + 1.0 mm (fix_08_311) and vice versa (fix_08_313) in the middle of the weld seam . The gap is 0.1 mm in all cases. (omnidirectional algorithm)

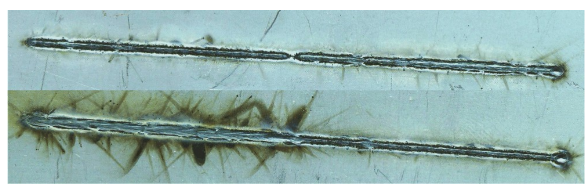

Fig. 14: Bottom sides of weld seams with 0.7 mm bottom sheet and thickness change from 0.7 mm to 1.0 mm (fix_08_311 top) and vice versa (fix_08_313 bottom) in the top sheet in the middle of the seam. (omnidirectional algorithm)

Direction independent experiments

The omnidirectional algorithm offers good stability and repeatability, as illustrated in Fig. 15. The feed rate of the whole weld seam was set to 5 m/min. Due to the limited dynamics of the mechanical axis of the xy-stage, the speed dropped to approximately 2 m/min in the circular section. The control system was able to follow the machine dynamics to maintain a suitable power level to achieve a sound weld [14].

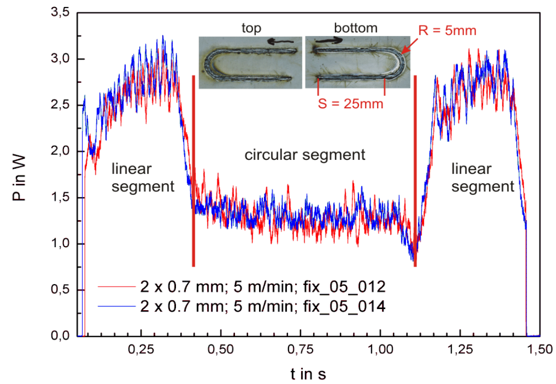

Fig. 15: Controlled full penetration weld of zinc coated steel. The material thickness is 2 x 0.7 mm with a gap of 0.1 mm in both cases. The weld seam starts with a 25 mm linear segment followed by a 180° circle with a radius of 5 mm and ends after another linear segment of 25 mm length [14].

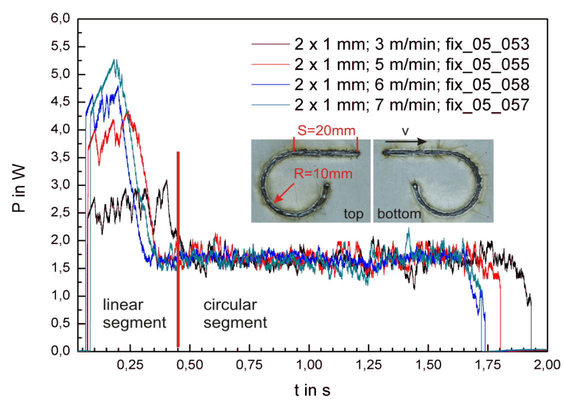

Fig. 16: Controlled full penetration weld of zinc coated steel. The material thickness is 2 x 1 mm with a gap of 0.2 mm in all cases. The weld seam starts with a 20 mm linear segment followed by a 270° circle with a radius of 10 mm [14].

A comparable test was performed to have speed steps with different heights. Fig. 16 shows results of the test where the linear segment was welded with different speeds between 3 m/min and 7 m/min. In the successive circular section the speed dropped to approximately 2 m/min. The control system was able to reach the full penetration in the linear segment automatically and to reduce the power to a suitable value for the circular section. The repeatability was very high as can be seen in Fig. 16 where the power level in the circular section is almost the same for all experiments [14].

Improvements in progress

This chapter describes improvements that are currently in development. Most of the current limitations are no principle limitations rather than limitations of the current way of implementation.

Line energy

One very important characteristic of a welding process is the line energy placed in the work piece. Compared to an uncontrolled full penetration welding process, the line energy of the controlled process should be equal or lower.

With the current implementation of the control system this is true for stack heights up to 3.2 mm. As Fig. 17 illustrates, the line energy of the controlled process is higher compared to the uncontrolled process, for stack heights above 4 mm.

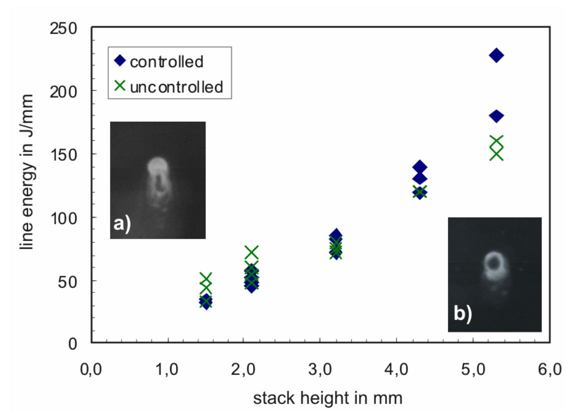

Fig. 17: Line energy over stack height for controlled and uncontrolled processes. Sub picture a) camera image at 9 m/min, b) camera image at 3 m/min.

This is not a principle limitation of the system. As sub picture b) in Fig. 17 clearly shows a full penetration hole, the problem is the image processing algorithm. There are too much false negative detections (the full penetration hole is present but not detected) on this shape of the interaction zone. This is due to the fact that the algorithm is developed and optimized for higher welding speeds, where the interaction zone has an elongated shape like in sub picture b) of Fig. 17. This problem will be fixed in future versions of the image processing algorithm.

Large step in feed rate

Due to the limited power gradients that can be generated by the control system there has to be critical acceleration of the feed rate, which cannot be controlled without a loss of penetration.

Paper published in Proc. of 28th International Congress on Applications of Lasers & Electro-Optics (ICALEO 2009

To demonstrate the effect of the power gradient on this, some experiments with 2 x 0.7 mm steel sheets were carried out. The feed rate was changed from 3 m/min to 9 m/min with an acceleration of 4 m/s².

Fig. 18 shows the curves of the laser power for three different limitations of the power gradient. The measured effective control speeds were 17 kW/s, 30 kW/s and 40 kW/s. Only with the effective control speed of 40 kW/s it was possible to maintain the full penetration state over the whole weld seam, see Fig. 19.

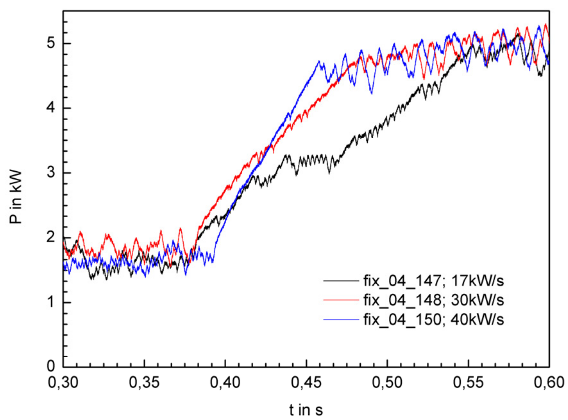

Fig. 18: Laser power gradient for a speed step from 3 to 9 m/min with an acceleration of 4 m/s². The maximum control speed is limited to three different values.

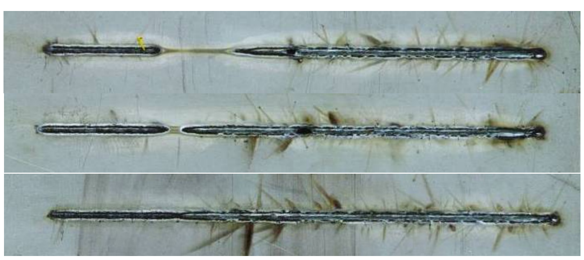

Fig. 19: Bottom sides of the corresponding weld seams. Control speeds from top to bottom: 17 kW/s, 30 kW/s and 40 kW/s.

For higher speed steps with the same acceleration, the 40 kW/s will not be sufficient, since the calculated necessary power gradient for this configuration is 120 kW/s. Thanks to the inertia of the process, the full penetration was maintained in this experiment despite the slow control speed.

Large step in material thickness

The same problem can occur in experiments with a step in the material thickness. Since the gradient of the thickness change is virtually infinite, only the inertia of the process ensures a constant full penetration at the bottom side of the work piece.

As shown in previous chapters, a constant full penetration can be achieved with a step from 0.7 mm to 1.5 mm in the top sheet at a feed rate of 6 m/min.

A limiting case for this behaviour is a step in the top sheet from 0.7 mm to 2.0 mm at a feed rate of 4 to 6 m/min. Fig. 20 shows the power gradient for this border case. The rise times of 84 ms respectively 86 ms are too long to ensure the full penetration over whole weld seams, as shown in Fig. 21.

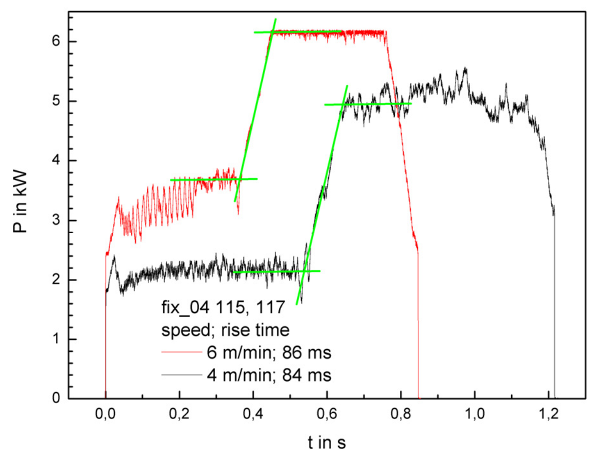

Fig. 20: Laser power gradient for a step in the material thickness of the top sheet from 0.7 mm to 2.0 mm. At welding speeds of 4 and 6 m/min.

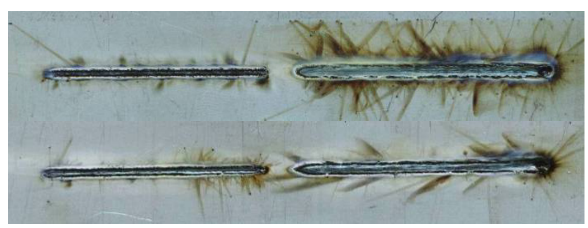

Fig. 21: Bottom sides of the corresponding weld seams. Rise times of the laser power were 84 and 86 ms. Top: fix_04_115, bottom: fix_04_117.

Gap size between the joining partners

To test the ability of the control system to deal with variable gap sizes between the sheets, some tests were done with opening gaps from 0.0 mm to 0.6 mm at material thicknesses of 2 x 0.7 mm.

Fig. 22 shows the graph of the controlled laser power for opening gaps. The gap has virtually no influence on the controlled laser power and the full penetration was ensured over the whole weld seam. Sample fix_04_166 suffered a "false friend" from the middle of the process. But the difference in the behaviour of the laser power was not very significant, which makes it hard to detect the "false friend".

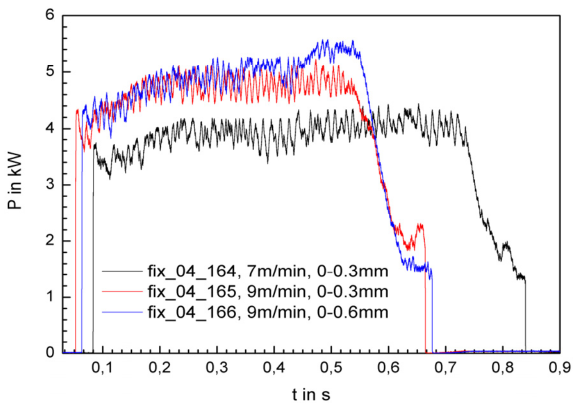

Fig. 22: Opening gap at 2 x 0.7 mm material and different feed rates.

Conclusion

The closed loop control system for full penetration laser welding processes proposed in former publications was extended with a new algorithm for direction independent image processing. With this new omnidirectional algorithm running on CNN hardware, it was possible to reach control frequencies of up to 7 kHz.

The major benefit for the laser welding process is a robust and fast contour detection of the rapidly changing full penetration hole. Based on this contour detection, an instant feedback signal for the laser power is generated. In that sense, the system marks the step from image based process monitoring to closed loop control systems which maintain the desired state of the process under a larger range of parameters. As demonstrated, the control system can handle different feed rates as well as variable thickness of the joining partners. These benefits are now available for arbitrary welding trajectories as shown in this paper.

Furthermore, the paper shows that the control system was stable in all situations in the sense that it always returned to the full penetration state. Limitations are mainly the limited power gradients, which can be a problem for large steps in the material thickness or high accelerations in the feed rate. These limitations can be avoided by using either a higher control frequency or a higher power step per frame. The problem of the line energy at high thicknesses and a prospect to overcome this problem were also described. The system is robust against variable gaps but the "false friend" could not be detected easily.

The CNN-based control system has proved its ability to meet the requirements for real-time high speed camera based process control in laser welding. In further experiments and projects, the system will be improved to cover a wider variety of quality features and other processes.

Acknowledgement

Most of the results were obtained within the project "Analoge Bildverarbeitung mit zellularen neuronalen Netzen (CNN) zur Regelung laserbasierter Schweißprozesse (ACES)" funded by the "Landesstiftung Baden-Württemberg".

Abbreviations

Table 1: Abbreviations and symbols

2D	Two dimensional
A/D	Analog/Digital Converter
β	Optical Magnification
CIF	Common Intermediate Format
CNN	Cellular Neural Network
f	Focal length in mm
FPGA	Field Programmable Gate Array
I/O	Input/Output
IC	Image Centre
IZC	Interaction Zone Centre
MULT	Multiplier Unit
NC	Numerically Controlled
P	Laser Power in W
PFO	Programmable Focussing Optics
PWM	Pulse Width Modulation
ROI	Region of Interest
SIMD	Single Instruction Multiple Data
t	Time in s
v	Feed rate in m/min
Yb:YAG	Ytterbium:Yttrium-Aluminium-Garnet

References

[1] A. Blug, F. Abt, L. Nicolosi, F. Dausinger, H. Höfler, R. Tetzlaff, R. Weber: CLOSED LOOP CONTROL OF LASER WELDING PROCESSES USING CELLULAR NEURAL NETWORK CAMERAS: MEASUREMENT TECHNOLOGY. Proc. of 28th International Congress on Applications of Lasers & Electro-Optics (ICALEO 2009), 2009, Orlando, Florida, USA

[2] Leon O. Chua, Fellow, IEEE, and Lin Yang, student member, IEEE, "Cellular Neural Networks: Theory", IEEE TRANSACTIONS ON CIRCUITS AND SYSTEMS, VOL. 35, NO. 10, OCT. 1988.

[3] Abt, F.; Nicolosi, L.;Carl, D.; Blug, A.; Geese, M.; Dausinger, F.; Deininger, C.; Höfler, H.; Tetzlaff, R.: CLOSED LOOP CONTROL OF LASER WELDING PROCESSES WITH CELLULAR NEURAL NETWORK (CNN) CAMERAS, Proc. of the 27th International Congress on Applications of Lasers & Electro-Optics (ICALEO 2008), 2008, Temecula, CA, USA, 817-825.

[4] Blug, A.; Carl, D.; Höfler, H.; Abt, F.; Geese, M.; Tetzlaff, R.: Pixelparallele Bildverarbeitung mit CNN zur Regelung von Laserschweiß-prozessen, VDI-Berichte, Sensoren und Messsysteme 2008, Vol. 2011, 2008.

[5] F. Corinto, M. Gilli and P.P. Civalleri, Dipartimento di Elettronica, Politecnico di Torino, Corso Duca degli Abruzzi 24, I-10129 Torino, Italy, On stability of full range and polynomial type CNNs, in Proc. of the 7th IEEE International Workshop on Cellular Neural Networks and their Applications, pp.33-40.

[6] S. Kaierle, P. Abels, G. Kapper, C. Kratzsch, J. Michel, W. Schulz, R. Poprawe: State of the Art and New Advances in Process Control for Laser Materials Processing. Proc. of 20th International Congress on Applications of Lasers & Electro-Optics (ICALEO 2001), Orlando, Florida, USA, October 2001.

[7] Fabbro, R.; Coste, F.; Goebels, D.; Kielwasser, M. (2004) Study of Nd-YAG Welding of Zn-Coated Steel Sheets, in Proceedings of the 23nd International Congress on Applications of Lasers and Electro-Optics, ICALEO 2004, San Francisco, USA.

[8] Bardin, F.; Cobo, A.; Lopez-Higuera, J.; Collin, O.; Aubry, P.; Dubois, T.; Högström, M.; Nylen, P.; Jons-son, P.; Jones, J.; Hand, D. (2004) Process Control of Laser Keyhole Welding, in Proceedings of the 23nd International Congress on Applications of Lasers and Electro-Optics, ICALEO 2004, San Francisco, USA.

[9] Company Anafocus, Avd. Isaac Newton s/n, Pa-bellón de Italia, Ático Parque Tecnológico Isla de la Cartuja, 41092 Sevilla, Spain.

[10] L. Nicolosi, R. Tetzlaff, F. Abt, A. Blug, H. Höfler, D. Carl, "New CNN based algorithms for the full penetration hole extraction in laser welding processes", IEEE International Symposium on Circuits and Systems ISCAS, May 24-27 2009, Taipei, Taiwan.

[11] Nicolosi, L.; Tetzlaff, R.; Höfler, H.; Blug, A.; Carl, D.; Abt, F.: Omnidirectional Algorithm for the Full Penetration Hole Extraction in Laser Welding Processes, in Proceedings of the European Conference on Circuit Theory and Design ECCTD 2009, Antalya, Turkey.

[12] M. Geese, R. Tetzlaff, D. Carl, A. Blug, H. Höfler, F. Abt, (2008) "Feature Extraction in Laser Welding Processes", in Proc. of the 11th International Workshop on Cellular Neural Networks and their Applications CNNA 2008, Santiago de Compostela, Spain.

[13] Abt, F.; Nicolosi, L.; Blug, A.; Dausinger, F.; Tetzlaff, R.; Höfler, H.: CNN-Cameras for Closed Loop Control of Laser Welding – Experimental Results and Prospects. Proceeding of the Lasers in Manufacturing (LIM) 2009, AT-Fachverlag, Munich, Germany.

[14] Abt, F.; Blug, A.; Nicolosi, L.; Dausinger, F.; Höfler, H.; Tetzlaff, R.; Weber, R.: Real Time Closed Loop Control of Full Penetration Keyhole Welding with Cellular Neural Network Cameras. Proceeding of the Laser Advanced Materials Processing (LAMP) 2009, Kobe, Japan.

Meet the Authors

Dipl.-Ing. Felix Abt – Diploma in Mechatronics (Automatisierungstechnik in der Produktion) at the University of Stuttgart, Germany. Working on a Ph.D.-thesis in the field of process diagnostics at the Forschungsgesellschaft für Strahlwerkzeuge (FGSW) since March 2006.